

2.C Effects of Non-Maxwellian Electron Populations in Non-LTE Simulations of Laser-Plasma Thermal Transport and Implosion Experiments

Spectrally and spatially resolved x rays are widely used diagnostics for high-temperature plasmas in laser-driven experiments. The relatively small time scales and small optical depths that occur often require a non-LTE (local thermodynamic equilibrium) analysis of atomic phenomena, and the relatively long mean free path of the most energetic electrons can make non-Maxwellian electron energy distributions relevant to the interpretation of the diagnostic signals. Just as deviations from a Planck photon spectrum occur in radiative transfer problems when photon optical depths are comparable to configurational scale lengths, small deviations from Maxwell-Boltzmann (MB) electron distributions can occur in small, transient laser-driven plasmas.

In this work, the long mean-free-path electrons are described by an MB distribution at a temperature T_h comprising a number fraction ϵ of the total electron density. This “hot” component and the main population at the “cold” temperature T_c form a bi-Maxwellian distribution that is sufficiently general to study the most important effects of hot electrons on the bulk ionization state of plasmas and on their x-ray diagnostics. The most likely sources of hot populations in a cold background are suprathermal electrons from resonant absorption and high-energy electrons from an approaching heat front or from a hot, compressed target core. This report will not consider the source of hot electrons but will examine the sensitivity of x-ray emission to the presence of an assumed hot-electron population. The effect of a small, non-Maxwellian electron population on atomic process rates is considered in the interpretation of two kinds of experiments.

The first kind of experiment discussed is the burn-through, thermal transport experiment in which x-ray lines are emitted from highly ionized medium-Z atoms of a metal layer when a laser-driven heat front has penetrated an overcoated plastic layer of a given thickness. The “turn-on” of a particular spectral feature is interpreted in these experiments as a signal that a particular isotherm of the heat front has arrived at the metal layer. Hydrodynamic simulations of previous experiments^{1,2} generally reproduced the observed penetration depths using thermal transport models consisting of the diffusive Spitzer-Härm transport model³ with a maximum allowed thermal flux F_{\max} equal to a fraction f of the free-streaming electron energy flux

$$F_{\max} = f n_e k T_e (k T_e / m_e)^{1/2}, \quad (1)$$

where the “flux-limit parameter”⁴ f lies within the range $0.01 \leq f \leq 0.1$. Recent experiments at LLE, however, have indicated penetration significantly deeper than can be calculated using the usual flux-limit formalism.^{5,6} This report considers the extent to which this apparent deep penetration can be attributed to the turn-on of the signature line at a relatively low temperature well ahead of the heat front, where the

electron energy distribution is augmented by a small population of higher-energy electrons. Such a population could originate in the hot, laser-heated plasma and penetrate deep into the colder part of the plasma due to their relatively long mean free paths.

The second kind of experiment to be considered is the implosion of glass microballoons diagnosed in part by x-ray microscope images.⁷ The time-integrated image of such an implosion seen in the 2- to 6-keV range is formed primarily by the recombination continuum from bare and H-like Si ions. The most prominent features in such images are an outer ring formed by the heat-front dwelling at its point of maximum excursion toward the center of the target and a central disc formed by emission from the inner surface of the glass shell as it is heated by the low-Z (DT) fill gas at maximum compression.

Numerically simulated images show considerable sensitivity to parameters such as the flux-limit parameter and the partition of laser energy into thermal and suprathermal electrons. By comparing these simulated images to the actual images, limits on these parameters can be set.⁷ However, we find that the intensities of the inner feature are particularly sensitive to small ($\leq 1\%$ by number) populations of hot (energy \geq few keV) electrons through their effect on atomic ionization and excitation rates; thus, the non-Maxwellian distribution can modify inferences made regarding the thermal flux inhibition and energy partitioning.

Line Turn-On in Non-Maxwellian Plasmas

To illustrate the effect of a small, hot-electron population on lowering the temperature for line emission, we calculate Lyman- α emission from an aluminum plasma, assuming collisional-radiative equilibrium with atomic ionization and transition rates modified for a non-Maxwellian electron spectrum. For the purposes of this report, a bi-Maxwellian distribution⁸ of the form

$$f_{BM}(v, \epsilon, T_c, T_h) = (1 - \epsilon)f_{MB}(v, T_c) + \epsilon f_{MB}(v, T_h) \quad (2)$$

will suffice. This distribution is a linear combination of MB distributions evaluated at the hot T_h and background T_c temperatures, with ϵ being the number fraction of electrons in the hot population. Collisional ionization, excitation and de-excitation, and radiative recombination rates for MB distributions are proportional to MB-weighted velocity integrals of their respective cross sections

$$R_{MB}(T) \propto \int \sigma(v) v f_{MB}(v, T) d^3v, \quad (3)$$

so that the bi-Maxwellian rates are also linear combinations of MB rates,

$$R(\epsilon, T_c, T_h) = (1 - \epsilon) R_{MB}(T_c) + \epsilon R_{MB}(T_h). \quad (4)$$

The most significant effect of the hot component on the ion populations is through the collisional ionization and excitation rates in which the most important temperature-dependent factor at the threshold of emission is the exponential term

$$R_{\text{MB}}(T) \sim \dots e^{-\chi/kT}, \quad (5)$$

where χ is the relevant excitation or ionization energy. At $T \sim 400$ eV, where the 1.7-keV Si Lyman- α line is seen, this exponential is of the order of 10^{-2} for the needed excitation. For $kT_h \geq \chi$, this factor is nearly unity, so that a 1% hot population is as effective as the entire cold population in driving the ionization. Since the threshold exponential is near unity for any T_h value in excess of the threshold energy, the effect of the hot population will be relatively insensitive to the value of T_h .

The ions in the model used here are treated in the hydrogenic approximation.⁹ Only singly excited states are considered, with the active electron orbiting in the field of a screened nucleus whose effective charge is calculated by subtracting the screening contribution of each core electron from the nuclear charge.¹⁰ All ionization species are included in the population set. Excited states through principal quantum number $n = 4$ are included in the hydrogen-, helium-, and lithium-like species. States are specified by principal quantum number only; the sublevels are assumed to be degenerate and equally populated. Continuum lowering of ionization energies is calculated according to the Stewart-Pyatt model.¹¹ Dielectronic recombination is not considered; it should have only a negligible effect on the ionic populations at the high densities ($n_i \geq 10^{20} \text{ cm}^{-3}$) examined.¹²

The possible effect of the hot component of the electron energy distribution on the appearance of the Lyman- α line from the Al layer of a target can be determined from the steady-state solution to the population equations containing these rates. The results shown in Fig. 22.17 give the relative population of the Al Lyman- α -emitting state,

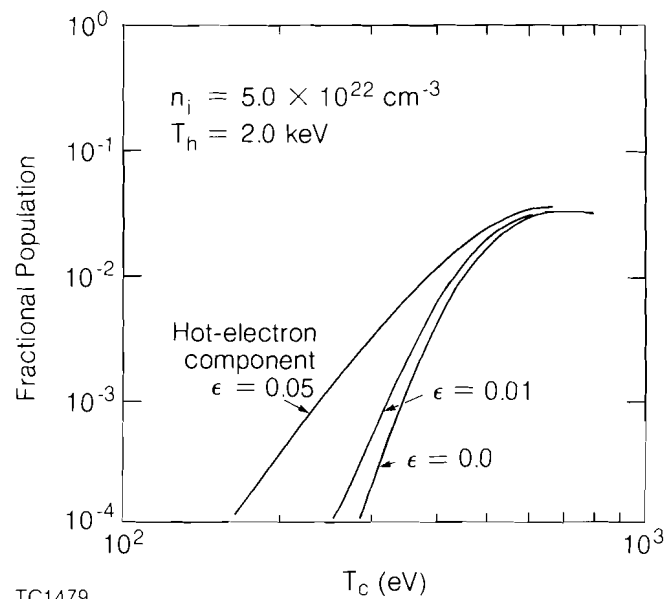


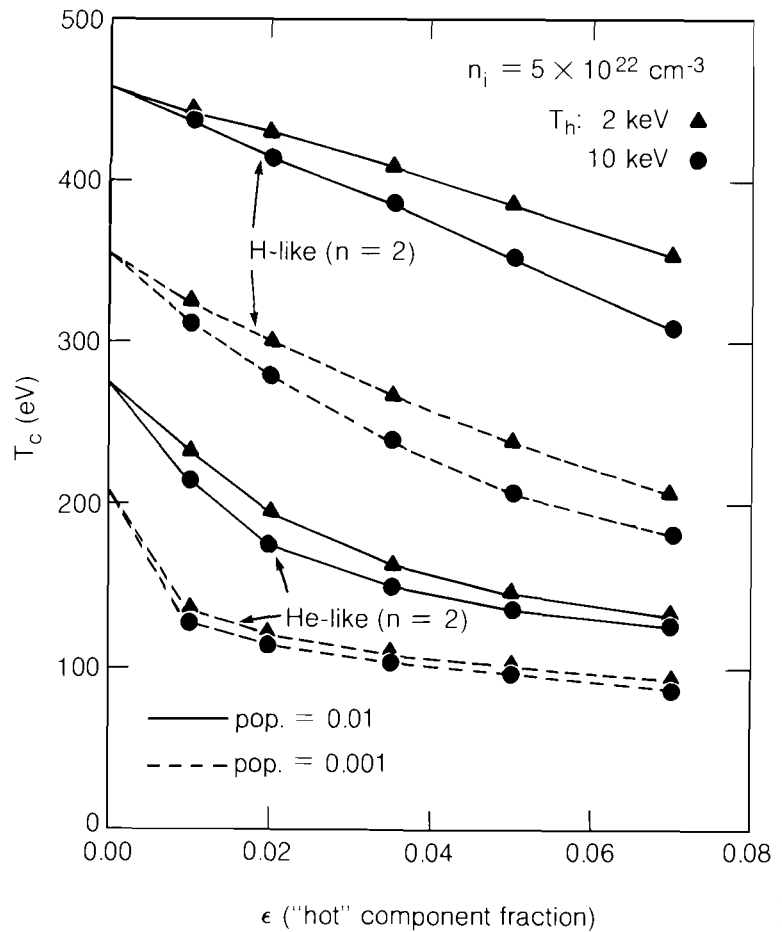
Fig. 22.17

The steady-state fractional population of the Lyman- α -emitting ($n = 2$) H-like species for optically thin conditions plotted as a function of T_c for various ϵ values. The density assumed, $n_i = 5.0 \times 10^{22} \text{ cm}^{-3}$, is representative of conditions expected at the foot of the heat front. At marginal turn-on temperatures, $T_c \sim 300\text{--}400$ eV, significant changes in the emitting population result from hot-electron fractions at $\sim 1\%$ level.

Fig. 22.18
 The background temperature T_c at which a fractional population of the Lyman- α (H-like, $n=2$)- or helium- α (He-like, $n=2$)-emitting species would reach values of 0.01 (—) or 0.001 (-----) is plotted as a function of the hot-electron population fraction ϵ . The plasma conditions are the same as assumed in Fig. 22.17. The $T_h = 2$ -keV (\blacktriangle) and 10-keV (\bullet) results are remarkably similar. Given a T_h value in this range of values well in excess of the relevant ionization energies, hot-electron populations at the 2–5% level can lower the background temperature value required to create these emitting-state populations of the order of 100 eV.

plotted as a function of the background temperature for an Al plasma at an ion density close to the solid density of $6.0 \times 10^{22} \text{ cm}^{-3}$, typical of what might be found ahead of the heat front. At a background temperature of 400 eV the population is near its peak value, and it drops rapidly at lower temperatures. The curves for additions of 1% and 5% 2-keV electrons show that these percentages of hot electrons do increase the emitting populations by significant factors. Thus, the background temperature at which a given population is reached can be reduced by adding a small hot-electron population.

The effect of the hot-electron population in lowering the background temperature at which a given emitting population exists is shown more clearly in Fig. 22.18. Curves representing the background temperature value at which either a 1% or 0.1% abundance of the H-like Lyman- α - or helium- α -emitting states occurs are plotted as functions of the hot-electron population fraction ϵ . The results for hot-electron temperatures of 2 keV and 10 keV are remarkably similar. This confirms indirectly the conjecture made earlier that the results should be relatively insensitive

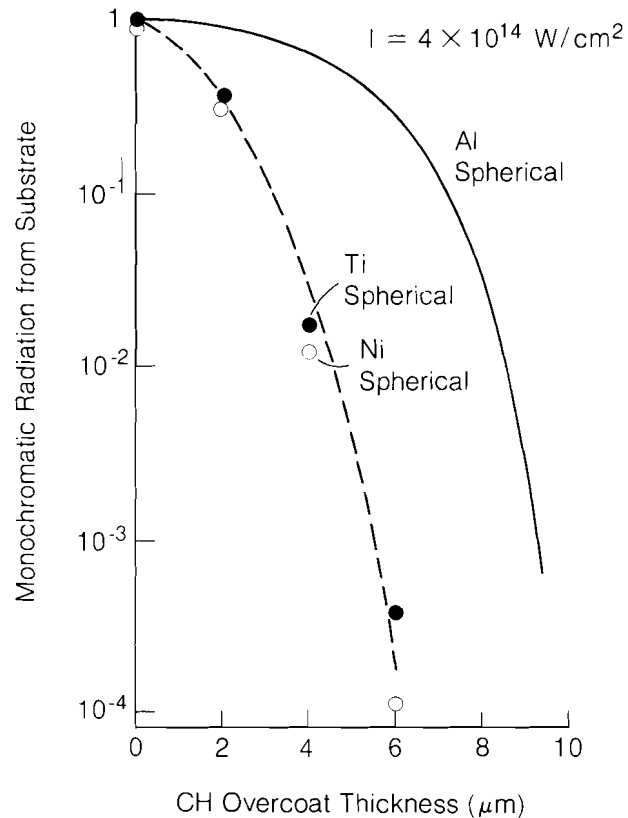


TC1481

to changes in kT_n well above threshold energies. It is seen that values of ϵ of 2–5% are sufficient to reduce the T_c value for a given population by about 100 eV.

Burn-Through Experiments

One experimental result that raises the possibility of non-Maxwellian effects on atomic transition rates is illustrated by the burn-through results shown in Fig. 22.19 for $\lambda_L = 1054\text{-nm}$ illumination on various CH coating thicknesses over various substrate materials.⁵ Similar results have been obtained recently with $\lambda_L = 351\text{-nm}$ illumination.⁶ The curves represent normalized intensities of specific emission lines. The CH thickness at which a given curve drops off by 10% can be taken as the penetration depth of a particular heat-front isotherm. The Al curves give the H-like Lyman- α intensity at 1.73 keV, which is expected to first appear at temperatures near 450 eV. The Ti and Ni curves representing their He-like $2^1P\text{-}1^1S$ resonance lines at 4.75 keV and 7.8 keV, respectively, correspond similarly to the arrival of the $\sim 1.0\text{-keV}$ and $\sim 1.5\text{-keV}$ isotherms.



E3291

Fig. 22.19

Normalized curves showing the cutoff of the time-integrated line emission from various substrates with increasing CH overcoat thickness at constant-incident intensity of $4 \times 10^{14} \text{ W/cm}^2$ under spherical illumination.⁵ The aluminum curve shows the Lyman- α intensity that is expected to appear with the arrival of the 400-eV isotherm at the substrate. The intensities of the $2^2P\text{-}1^1S$ resonance lines of He-like titanium and nickel signal temperatures of $\sim 1.0 \text{ keV}$ and $\sim 1.5 \text{ keV}$, respectively.

The penetration of the 400-eV isotherm observed in the spherically illuminated Al experiments exceeds numerically simulated penetrations by roughly a factor of 3 for a broad range of flux-limit parameter values.⁵ The penetration depths of the higher temperature isotherms

signaled by the Ti and Ni emission are much closer to predicted values. One straightforward interpretation of this result considered at the time this experimental result was reported is that flux-limited diffusion theory is inapplicable to this problem.⁵ There might exist a low-temperature precursor or "foot" on the heat front that cannot be simulated without a nonlocal multigroup electron transport model. This foot is formed by the higher-energy, long mean-free-path electrons from behind the heat front penetrating into colder background material at a temperature T_c . A possible explanation of the premature turn-on of the Al emission is that the emission comes from substrate material at a background temperature much less than 400 eV, where the ionization and excitation of the aluminum is driven by the small hot-electron population. The likelihood of this explanation will be considered in terms of whether a plausible hot population can excite a sufficiently large population of emitting ions at values of T_c much less than the nominal 400-eV turn-on temperature.

The results discussed previously and illustrated in Fig. 22.19 tend to reinforce the earlier interpretations of the burn-through experiments based on Maxwellian atomic rates. A lowering of the Lyman- α turn-on temperature by 100 eV is probably not sufficient to account for the burn-through depths observed. Even a 1% hot-electron population, which would not lower the turn-on temperature sufficiently, would contain of the order of 10% of the plasma energy. Hot-electron populations of this size beyond the heating front are far larger than what appears to be plausible, based on available simulations of suprathreshold electron transport and multigroup Fokker-Planck simulations of thermal transport.¹³ These results suggest that the magnitude of the non-Maxwellian effect is not large enough to explain the burn-through results and that other physical mechanisms must be sought.

Images of Implosions

The x-ray image of an ablatively imploded DT-filled glass microballoon can be particularly sensitive to hot-electron populations when the temperature of the inner part of the glass shell is very close to the threshold for strong x-ray emission. The image of the emission is a potentially sensitive diagnostic of implosion dynamics and thermal transport because small changes in the inner part of the shell near this threshold can have a large effect on the image. The source of hot electrons in the shell inner region would be electrons of the "tail" of the distribution in the hot DT.

One such implosion image of 3-keV emission has previously been reported.⁷ The image is formed primarily by the recombination continuum of the bare and H-like species of the silicon in the glass shell.

Theoretical simulations of the x-ray pinhole image of this implosion have been obtained by solving the equation of radiative transfer using the temperature and density history of the implosion calculated by the 1-D Lagrangian hydrocode *LILAC*.¹⁴ *LILAC* includes separate ion and electron temperatures, flux-limited thermal electron transport, multigroup suprathreshold electron transport, ray tracing of the incident laser light, and multigroup radiation transport with tabulated LTE opacities.¹⁵ Opacities and emissivities for the image simulation are calculated using

temperature and density information from the hydrocode solution, and atomic population information derived from the rate equations described earlier. The time-dependent atomic rate equations include K-shell photoionization and photoexcitation of the first two Lyman-series lines of the H-like and He-like species. Doppler line profiles are used at low densities, and Stark-broadened line profiles calculated by Hooper¹⁶ are used at higher densities.

Figure 22.20 shows the shell conditions near peak compression of a simulation of this implosion, obtained using a flux-limit parameter $f = 0.03$ and a suprathreshold-electron deposition fraction $\eta_s = 0.16$. The top plot shows the electron temperature and ion density of the shell, and the center plot shows the relative populations of the ground states of the bare, H-like, and He-like silicon species. The bottom plot illustrates the double-featured structure of the time-integrated image formed by the 3-keV emission from such an implosion. The intensity peaks in this image correspond with regions of relatively intense, recombination continuum emission in the plasma – at times near peak compression.

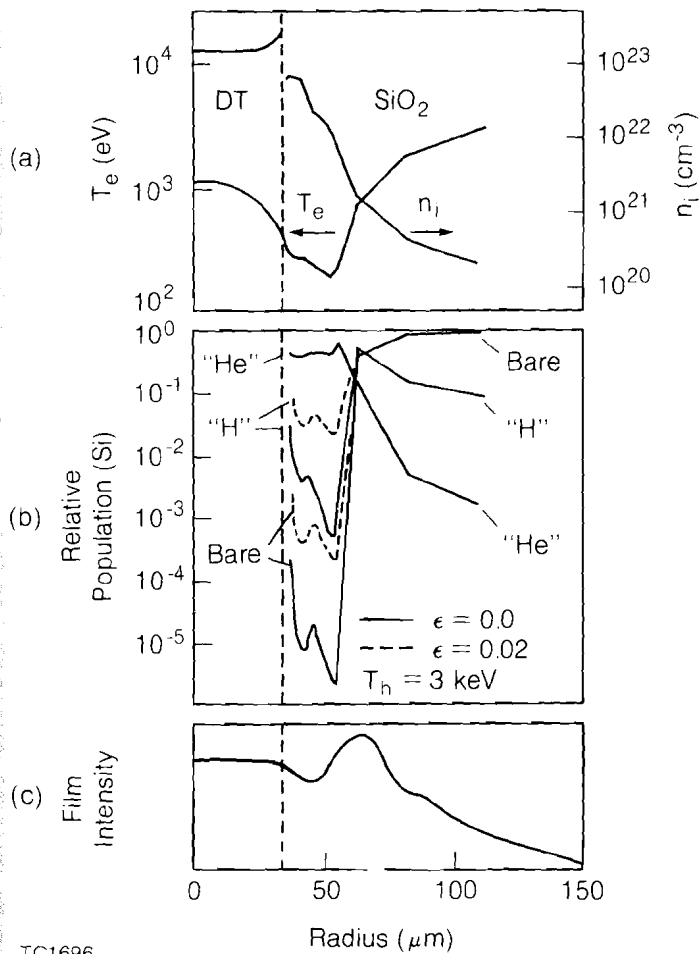


Fig. 22.20
 Simulated peak-compression conditions in the imploded microballoon at a time near peak compression. The time-integrated recombination emission that forms the image shown in (c) as a radial trace is emitted primarily in the ~ 200 -ps time interval when these peak conditions prevail. The temperature and density are plotted in (a), and the population fractions of the ground states of the three most highly ionized silicon species are plotted in (b). The dashed lines in (b) show how the primary emitting populations are raised by the presence of the 2% hot-electron population.

The higher emissivity results from high abundances of the H-like and bare species, from the high temperatures near the ablation front, and from the high temperature and density near the glass-DT interface.

Figure 22.21 shows several image simulations for this implosion. Similar image simulations were prepared from hydrocode results using other values of f and η_s . The solid curve in Fig. 22.21 is the non-LTE result based on Maxwellian atomic rates, and the dashed curve was obtained using LTE atomic populations. The limits $\eta_s < 0.20$ and $0.03 \leq f < 0.08$ have been inferred for this implosion based upon the resemblance of simulated LTE images to the densitometer trace, particularly in the occurrence of distinct inner and outer features that are comparable in intensity.⁷ The images shown in Fig. 22.21 were obtained assuming specifically $f = 0.03$. The close resemblance in shape between the LTE and non-LTE images in Fig. 22.21 was also obtained for other simulations based on plausible values of f and η_s . In non-LTE, nonstatistical balances of inverse processes and finite ionization rates tend to reduce the degree of ionization from that obtained in LTE. This accounts for the non-LTE image being less intense overall than the LTE image, but not for the similarity in structure between these two images. This similarity is probably fortuitous, but it nevertheless supports inferences drawn from comparisons of the observed image with the results of LTE image simulations.⁵

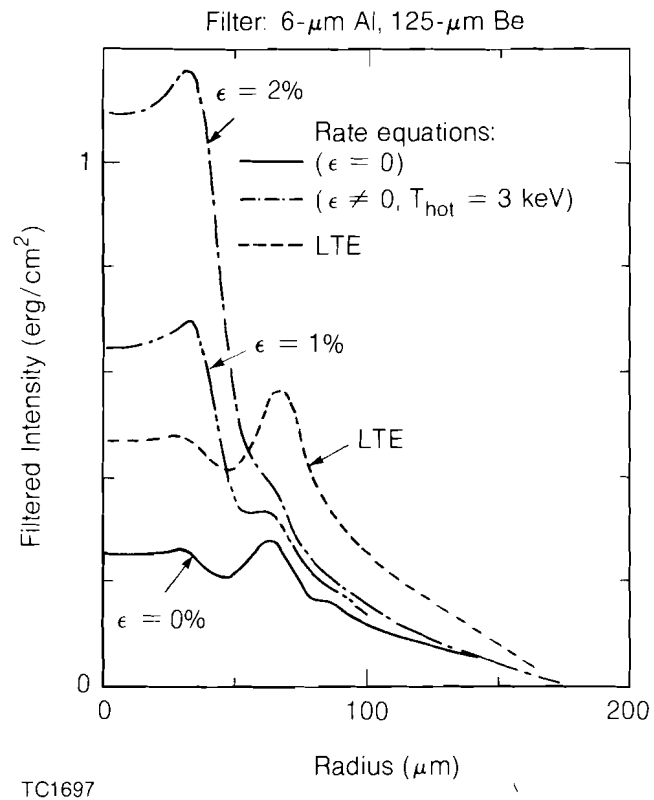


Fig. 22.21 Radial traces of the simulated pinhole image intensity from the microballoon implosion for various assumptions, including LTE atomic populations and various hot-electron fractions and energies. The hot electrons affect the inner feature most strongly since the background temperature there is relatively cool.

The two remaining image curves in Fig. 22.21 were obtained assuming various hot-electron populations. For convenience, the values of ϵ and T_h were assumed to be constant throughout the glass shell, but they only have a significant effect in the emitting region of interest. Since the shell material emitting the outer-feature radiation is already at $T_e \sim 1$ keV, the additional hot population has a negligible effect on this feature. The inner feature, however, is formed by emission from a 300-eV environment in which the small hot-electron populations affect the emitting populations markedly, as can be seen from the dashed curves in Fig. 22.20(b). This results in a significantly enhanced inner feature. The images obtained for value of $T_h = 3$ keV resemble the curves obtained for any value of T_h close to or above this value because of the threshold effect previously discussed.

The hydrocode simulation upon which the images in Fig. 22.21 are based used a flux-limit parameter of $f = 0.03$. The observed equal intensities of the inner and outer features correspond to a case intermediate between the $\epsilon = 0.0$ and $\epsilon = 0.01$; $T_h = 3$ -keV curves shown at roughly $\epsilon \approx 0.001$. A similar set of curves based on simulations using $f = 0.05$ gives a reasonably close resemblance to the observed image with $\epsilon = 0.0$. Assuming $f=0.08$ gives a much too intense inner feature, one could then take $f=0.05$ as a rough "best estimate," given the simplest hypothesis $\epsilon=0.0$. If it is only assumed that ϵ is non-negative, then $f = 0.05$ becomes an upper limit rather than an estimate. Significantly lower values of f cannot be ruled out without adequate upper limits on ϵ at 10^{-3} level.

It should be pointed out that changes in the shape of x-ray spectral lines can be expected from added hot electrons. The Si helium- β profile in Fig. 22.22 is a superposition of emission from the low-density corona and from the high-density compressed core. As seen in the simulated line profiles, the helium- β line acquires a Stark-broadened component from emission at high density as the hot electrons in the dense inner shell excite the relatively abundant He-like ground population (see Fig. 22.20). The few-percent hot-electron populations required in the inner shell in this example are not likely to occur, but if the inner temperature were higher, then a smaller fraction of hot electrons would be required to produce observable effects in the wings of the line.

Conclusion

This report serves in part as a preliminary assessment of the importance of non-Maxwellian electrons in interpreting x-ray diagnostics of laser-fusion experiments. If hot populations of more than at least a few percent are ever shown to be plausible, then hot-electron effects on line spectra from burn-through experiments will be an important consideration. The shape of x-ray images appears to be much more sensitive to hot electrons, perhaps sufficiently so to warrant a more detailed treatment of thermal electron transport in the simulation of images. These results are probably more significant as an assessment of the sensitivity of these diagnostics to given levels of hot-electron abundance, rather than as an assessment of the absolute importance of hot-electron effects. In view of the tentative state of thermal transport theory as applied to full simulations of these experiments, any speculation about the plausibility of a given hot-electron population level should also be regarded as tentative.

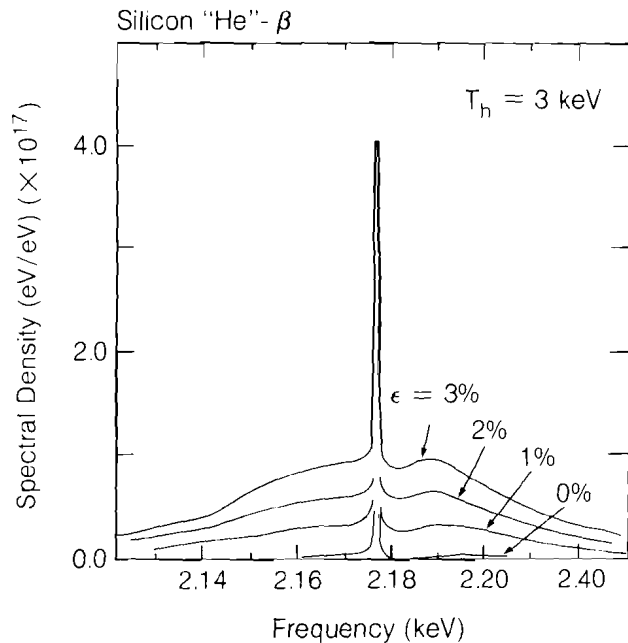


Fig. 22.22

Simulated time-integrated spectral intensity plotted near the Si helium-like β line. As the fractional population of $T_h = 3$ -keV electrons is increased, Stark-broadened emission from the dense inner shell increases.

ACKNOWLEDGMENT

This work was supported by the U.S. Department of Energy Office of Inertial Fusion under agreement number DE-FC08-85DP40200 and by the Laser Fusion Feasibility Project at the Laboratory for Laser Energetics which has the following sponsors: Empire State Electric Energy Research Corporation, General Electric Company, New York State Energy Research and Development Authority, Northeast Utilities Service Company, Ontario Hydro, Southern California Edison Company, The Standard Oil Company, and University of Rochester. Such support does not imply endorsement of the content by any of the above parties.

REFERENCES

1. B. Yaakobi, T. Boehly, P. Bourke, Y. Conturi, R. S. Craxton, J. Delettrez, J. M. Forsyth, R. D. Frankel, L. M. Goldman, R. L. McCrory, M. C. Richardson, W. Seka, D. Shvarts, and J. M. Soures, *Opt. Commun.* **39**, 175 (1981).
2. W. C. Mead *et al.*, *Phys. Fluids* **27**, 1301 (1984); A. Hauer *et al.*, *Phys. Rev. Lett.* **53**, 2563 (1984).
3. L. Spitzer and R. Härm, *Phys. Rev.* **89**, 977 (1953).
4. R. C. Malone, R. L. McCrory, and R. L. Morse, *Phys. Rev. Lett.* **34**, 721 (1975).
5. B. Yaakobi, J. Delettrez, L. M. Goldman, R. L. McCrory, R. Marjoribanks, M. C. Richardson, D. Shvarts, S. Skupsky, J. M. Soures, C. Verdon, D. M. Villeneuve, T. Boehly, R. Hutchison, and S. Letzring, *Phys. Fluids* **27**, 516 (1984).

6. LLE Review **17**, 32 (1983); B. Yaakobi, O. Barnouin, J. Delettrez, L. M. Goldman, R. Marjoribanks, R. L. McCrory, M. C. Richardson, and J. M. Soures, *J. Appl. Phys.* (to be published).
7. J. Delettrez, presented at the 14th Annual Anomalous Absorption Conference, Charlottesville, VA, 1984, paper G11; LLE Review **20**, 160 (1984).
8. R. Epstein, S. Skupsky, J. Delettrez, and B. Yaakobi, *Bull. Am. Phys. Soc.* **28**, 1219 (1983); J. P. Apruseze and J. Davis, *Phys. Rev. A* **28**, 3686 (1983).
9. H. Mayer, Los Alamos Report No. AECD-1870 (1947), quoted in G. C. Pomraning, *The Equations of Radiation Hydrodynamics* (Pergamon Press, New York, 1983), pp. 168-169.
10. J. C. Slater, *Phys. Rev.* **36**, 57 (1930), quoted in G. C. Pomraning, *op. cit.*
11. J. C. Stewart and K. D. Pyatt, *Astrophys. J.* **144**, 1203 (1966).
12. D. Salzmänn and A. Krumbein, *J. Appl. Phys.* **49**, 3229 (1978).
13. J. Delettrez (unpublished).
14. Earlier versions of *LILAC* are described in LLE Reports No. 16 (1973) and No. 36 (1976).
15. W. F. Huebner, A. L. Merts, N. H. Magee, and M. F. Argo, Report No. LA-6760, 1977 (unpublished).
16. R. J. Tighe and C. F. Hooper, *Phys. Rev. A* **17**, 410 (1978); C. F. Hooper (private communication).